

Improving leaf area index estimation accuracy of wheat by involving leaf chlorophyll content information

Zhulin Chen^{a,b}, Kun Jia^{a,b,*}, Xiangqin Wei^{c,*}, Yan Liu^c, Yulin Zhan^c, Mu Xia^{a,b}, Yunjun Yao^{a,b}, Xiaotong Zhang^{a,b}

^a State Key Laboratory of Remote Sensing Science, Faculty of Geographical Science, Beijing Normal University, Beijing 100875, China

^b Beijing Engineering Research Center for Global Land Remote Sensing Products, Faculty of Geographical Science, Beijing Normal University, Beijing 100875, China

^c Aerospace Information Research Institute, Chinese Academy of Sciences, Beijing 100101, China

ARTICLE INFO

Keywords:

Leaf area index
Leaf chlorophyll content
Sensitivity analysis
Vegetation index
Red-edge band

ABSTRACT

Red-edge band is widely used for LAI estimation as it is highly correlated to vegetation growth conditions. Canopy reflectance is affected by both vegetation biophysical and biochemical characteristics. However, estimating LAI using satellite reflectance data as input rarely considers the influence of leaf chlorophyll content (LCC). This study tested the hypothesis whether LAI estimation accuracy can be improved by involving LCC information. Firstly, the sensitivities of seven PROSAIL simulated Sentinel-2 bands to LAI and LCC were investigated, and related vegetation indices (VIs) were constructed using these sensitive bands (including LAI-sensitive VIs and LCC-sensitive VIs). Then, the LAI estimation model taking sensitive VIs as input and LCC estimation model taking sensitive VIs as input were generated by random forest regression algorithm. Finally, the improved LAI estimation model involving LCC information was proposed using three different methods: (1) PROSAIL simulated LCC, (2) simulated LCC with noise, and (3) functional equation of LCC. The results indicated that the three LCC information introducing methods all improved the LAI estimation accuracy, while using the functional equation of LCC (growth equation) performed best with RMSE of 0.736, which is 11.54% higher when compared to the basic LAI estimation model.

1. Introduction

Leaf area index (LAI) is defined as the ratio of total one-sided leaf area to the ground area (Chen and Black, 1992), which is a crucial indicator for characterizing the land surface vegetation states. LAI affects many biological and physical vegetation processes, such as photosynthesis and respiration (Chen and Cihlar, 1996), and has been widely used in the hydrological, crop yield and ecological models (Zhang et al., 2020; Xia et al., 2021) due to its ability to describe mass (e.g., water and carbon) and energy (e.g., radiation and heat) exchange between biosphere and atmosphere (Yan et al., 2019). Therefore, accurate LAI estimation is of great importance for a variety of earth systems, agriculture and ecological studies.

Remote sensing provides a faster and cost-effective method for LAI estimation over large areas. The traditional LAI estimation method using remote sensing data builds empirical statistical models based on

sensitive band reflectances, vegetation indices (VIs), or spectral transform values (Chen et al., 2020). Empirical methods are easily affected by the vegetation types, experimental locations, and sampling times. Therefore, empirical models show limited capabilities when applied to large-scale and multitype vegetation areas. In contrast, the physical-based methods have no such limitation because they consider various vegetation biophysical and biochemical parameters, and soil reflectances. However, the radiation transfer model (RTM) used in physical-based method requires many input parameters for accurate simulations. Therefore, the inversion of RTM is very difficult, and hybrid LAI estimation models have been widely used for LAI estimation (Sinha et al., 2020). By combining a physical model and machine learning algorithm, hybrid methods have advantages of both empirical and physical inversion algorithms.

The VIs are essential inputs for both statistical and hybrid models. For example, the normalized difference vegetation index (NDVI) is

* Corresponding authors at: State Key Laboratory of Remote Sensing Science, Faculty of Geographical Science, Beijing Normal University, Beijing 100875, China (K. Jia) and Aerospace Information Research Institute, Chinese Academy of Sciences, Beijing 100101, China (X. Wei).

E-mail addresses: chenzhulin@mail.bnu.edu.cn (Z. Chen), jiakun@bnu.edu.cn (K. Jia), weixq@aircas.ac.cn (X. Wei), liuyan@aircas.ac.cn (Y. Liu), zhanyl@aircas.ac.cn (Y. Zhan), xiamu@mail.bnu.edu.cn (M. Xia), yaoyunjun@bnu.edu.cn (Y. Yao), xtngzhang@bnu.edu.cn (X. Zhang).

<https://doi.org/10.1016/j.compag.2022.106902>

Received 27 December 2021; Received in revised form 15 March 2022; Accepted 20 March 2022

Available online 26 March 2022

0168-1699/© 2022 Elsevier B.V. All rights reserved.

widely used for LAI estimation (Hasegawa et al., 2010; Sinha et al., 2020). However, the Red-NIR band combinations easily suffer from saturation at moderate-to-dense canopies, which usually cause underestimation for moderate-to-high LAI values (LAI > 3) (Delegido et al., 2013). The reason is that NIR band reflectances increase rapidly due to scattering of light in intercellular volumes of leaf mesophylls (Dorigo et al., 2007), while red band reflectances exhibit fewer variations since they become saturated with high chlorophyll content. To improve the sensitivity to moderate-to-high LAI values, various new VIs have been developed in the past few decades. One solution is to attenuate the reflectance contrast between the red and NIR bands, such as modified simple ratio index (MSR) (Chen 1996). Although this method is effective for multispectral bands (e.g. Landsat-8) (Dong et al., 2020), it still shows a limited capability for reducing the underestimation phenomenon. During the past 20 years, the development of hyperspectral imaging sensors has provided plenty of narrow bands from visible to NIR wavelength (Delegido et al., 2013). The red-edge (RE) wavelength is discovered to be influenced by multiple scattering between leaf layers, and is strongly affected by LAI. Moreover, because the RE bands are sensitive to vegetation conditions, several studies have used them to formulate VIs and achieved more accurate LAI estimation in the moderate-to-high dense canopy regions (Brown et al., 2019). Therefore, a number of RE-based VIs, such as the red edge normalized difference vegetation (NDVIRE) and red edge chlorophyll index (CIRE), have been widely used for LAI estimation (Sibanda et al., 2019).

Although, the RE-based VIs have contributed to LAI estimation accuracy improvement, some concerns still need to be solved (George et al., 2018). Although the RE-based VIs developed using hyperspectral reflectances possess great potential, those narrow RE band-based VIs can hardly applied to large region because of the small amount of hyperspectral data. Fortunately, several spaceborne sensors that involve RE bands have been designed and launched, such as Rapid-Eye, WorldView-2, Sentinel-2 (S2), and Chinese GF-6. Among those sensors, the S2 Multispectral Instrument (MSI) provides the most detailed RE bands. Thus, it is of great significance to discuss the potential of improving LAI estimation accuracy by using S2 data. Other than VIs, another important but often ignored parameter is leaf chlorophyll content (LCC). It also has a great influence on RE band reflectance (Xie et al., 2018). The increase of LCC not only causes strong absorption in the red spectral wavelengths, but also leads to a shift in the RE band toward longer wavelengths (Herrmann et al., 2011). In recent years, some studies have attempted to reduce the effect of LCC change by excluding LCC-sensitive bands in LAI estimation (Sun et al., 2020). However, since it is impossible to fully separate the influence of these two parameters on reflectance, the effects of LCC changes are still nonnegligible for LAI estimation. Another disadvantage of the above method is that the canopy information provided by RS data is not fully used. Although LCC-sensitive bands are not recommended for LAI-sensitive VI modifications, they can be combined with LAI-sensitive VIs to increase the information on canopy status for LAI estimation. According to plant physiology studies (Dordas and Sioulas, 2008), photosynthesis which is directly influenced by LCC is one of the crucial factors for plant growth (including LAI enlargement). Those studies have indicated that LCC is also capable of characterizing the vegetation growth status and related to LAI. However, there is no obvious linear relationship between these two parameters. Fortunately, the development of machine learning algorithm provides an opportunity to solve complex nonlinear relationships between LAI and LCC. Therefore, based on the powerful nonlinear expression ability of machine learning algorithm, it is possible to adopt LCC information in characterizing the current state of LAI.

As discussed above, this study aims to test the hypothesis of improving LAI estimation accuracy of wheat by involving LCC information. To achieve this objective, two issues need to be resolved. Firstly, the basic LAI estimation model should be established using LAI-sensitive VIs. Secondly, since LCC information can be involved in various ways, the best LCC introducing form needs to be determined for LAI estimation

accuracy improvement.

2. Materials and methods

First, the PROSAIL (PROSPECT and Scattering by Arbitrarily Inclined Leaves (SAIL)) model was used to simulate the S2 multispectral reflectances and the corresponding LAI and LCC values (Fig. 1). Global sensitivity analysis was applied to identify LAI-sensitive bands and LCC-sensitive bands for VIs construction. To select the best VIs for LAI and LCC estimation, several VIs were calculated by different band combinations. LAI and LCC estimation models were established using the random forest regression (RFR) algorithm. Then, the model with the highest estimation accuracy was chosen as the basic LAI estimation model. Next, the LCC information with three introducing methods was added to the basic LAI estimation model, respectively. Finally, the best LCC introducing method and best LAI estimation model were determined.

2.1. Study area and field survey

The study area is located in Hengshui (115°10'E ~ 116°34'E, 37°03'N ~ 38°23'N), Hebei province of China. It has a temperate continental monsoon climate with an annual average temperature of 13.2°C and annual average precipitation of 642.1 mm. The climatic conditions and flat terrain with an altitude varying from 10 to 20 m (above sea level) are very suitable for the growing of wheat (*Triticum aestivum L.*) and maize (*Zea mays L.*). Field LAI measurements were conducted twice during the different growing stages of wheat using a LAI-2200C plant canopy analyzer (LI-COR Inc., Lincoln, Nebraska) (first: 29 March 2017 to 1 April 2017; second: 4 May 2017 to 6 May 2017). There were 22 sample sites with the size of 100 m × 100 m across 112 counties of Hengshui (Fig. 2). Five sample plots with the size of 30 m × 30 m were established at each sample site. Five measurements were taken in one plot, and the average value was calculated as the final LAI measurement for one sample plot. Therefore, there were a total of 220 ground measured LAI values during the whole survey period. However, only 218 LAI measurements could be used in this study due to cloud contamination of the remote sensing data.

2.2. Sentinel-2 data and preprocessing

As a part of the European Commission's Copernicus program, Sentinel-2A and Sentinel-2B were launched on June 23, 2015 and March 7, 2017, respectively. Those two satellites are in the same solar orbit and phased at 180° to each other. The MSI installed on the twin satellites provides images with a resolution of 10 to 60 m in 13 spectral channels (Drusch et al., 2012). In this study, seven visible and near-infrared bands (including Green, Red, RE1, RE2, RE3, NIR1, and NIR2) were used to construct VIs (Table 1). The Level-1C products of Sentinel-2 (Table 2) were selected, and the Sen2Cor processor in the Sentinel Application Platform (SNAP) toolbox was used for atmospheric correction. The bands with 10 m resolutions were resampled to 20 m, and adjacent images with the same acquisition dates were mosaicked.

2.3. Simulated data generated using PROSAIL model

Coupled by the leaf optical properties model PROSPECT and scattering by arbitrarily inclined leaves (SAIL), the radiative transfer model PROSAIL is widely used due to its high simulation accuracy and computing efficiency (Jia et al., 2016). By considering the non-Lambertian characteristics of soils, specular reflections of leaves, hot spot effect of vegetation canopies, and distributions of leaf inclinations, the PROSAIL model can accurately describe the reflection characteristics of vegetation canopies (Jay et al., 2017). Based on the field measurements and previous studies, the parameters of PROSAIL model as well as their ranges or values used in this study are shown in Table 3.

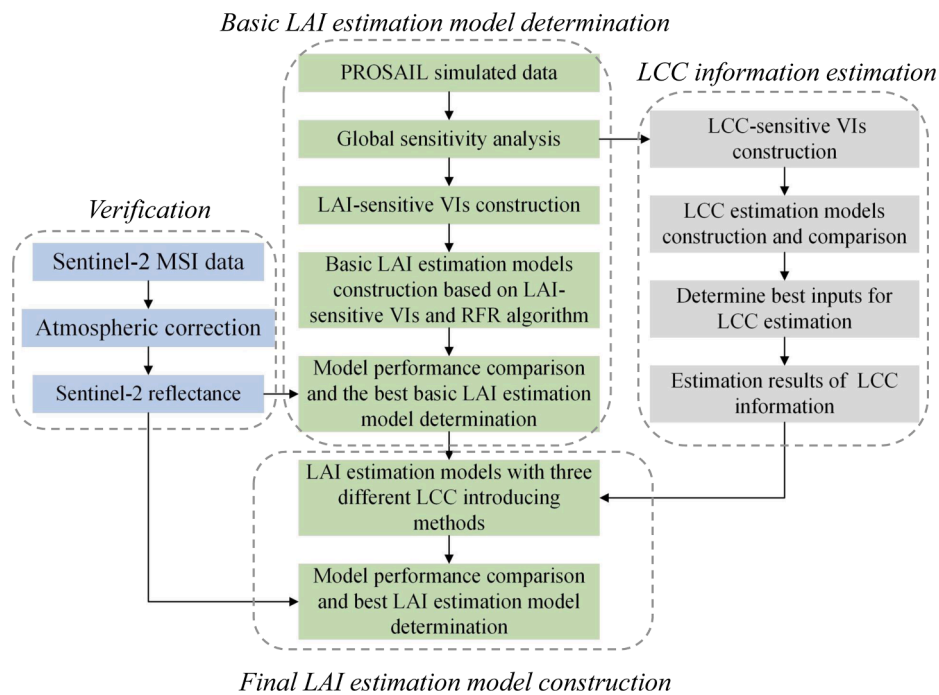


Fig. 1. Flow chart of this study.

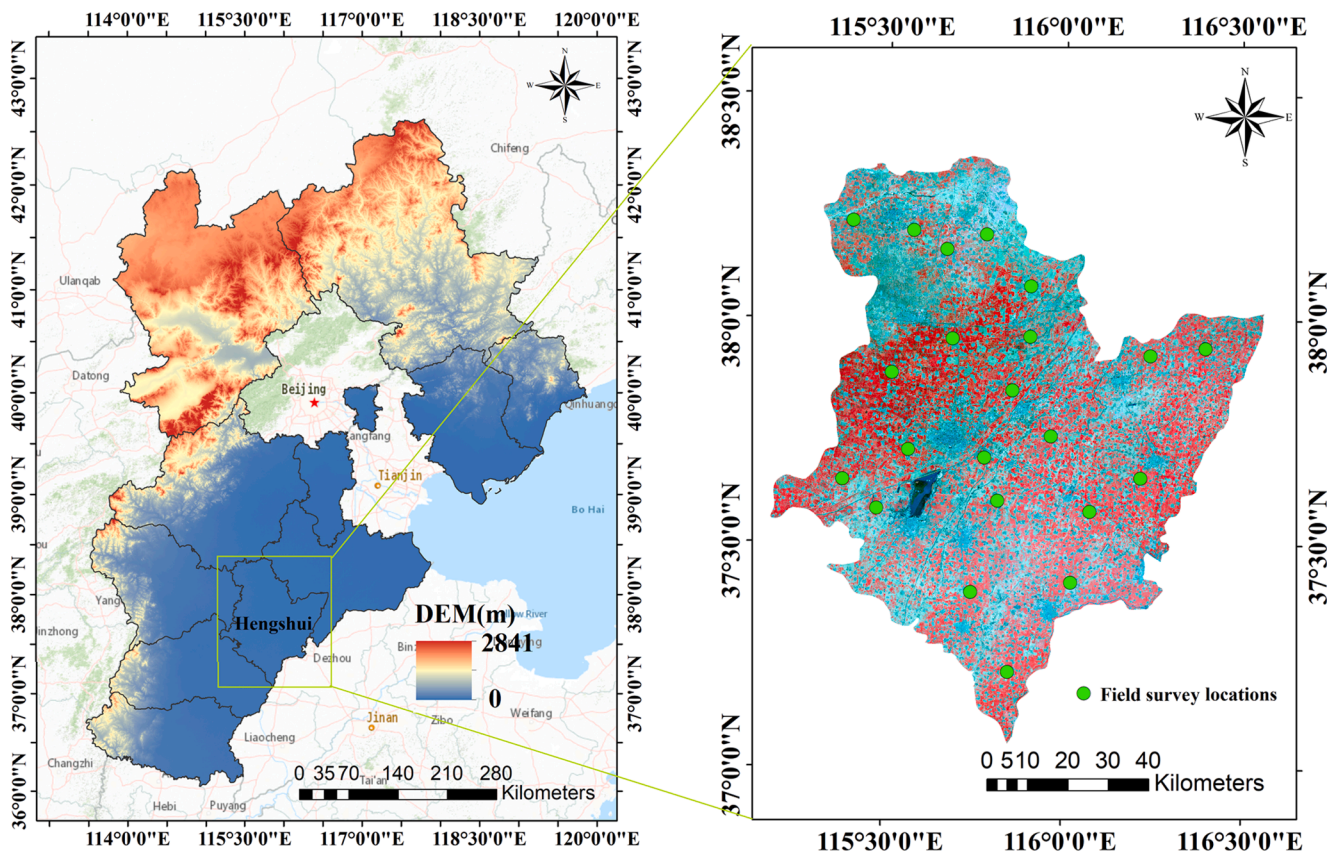


Fig. 2. Geographic location of the study area.

In addition, the soil reflectance is also an important input for the PROSAIL model. In this study, 5 soil reflectances were selected from the field measurements in Hengshui. After simulation, the canopy reflectance in each band was simulated by using the spectral response function of Sentinel-2. Since the reflectance extracted from the Sentinel-2

data contains uncertainties, white Gaussian noise at a level of 1% was added to the simulated data. In total, 150,000 simulated canopy reflectance along with their corresponding LAI and LCC values were generated using the PROSAIL model.

Table 1
Seven Sentinel-2 MSI band information.

Band name	Sentinel-2A		Sentinel-2B		Resolution (meters)
	CW (nm)	BW (nm)	CW (nm)	BW (nm)	
Green	560.0	35	559.0	35	10
Red	664.5	30	665.0	30	10
RE1	703.9	15	703.8	15	20
RE2	740.2	15	739.1	15	20
RE3	782.5	20	779.7	20	20
NIR1	835.1	115	833.0	115	10
NIR2	864.8	20	864.0	20	20

Notes: CW represents central wavelength; BW represents band width.

Table 2
Images used in this study.

Sensing Time	Tile Number
29 March 2017	50SLG, 50SLH, 50SMG, 50SMH
28 April 2017	50SLG, 50SLH, 50SMG, 50SMH

Table 3
Ranges or values of parameters used in the PROSAIL model.

Model	Parameters	Range (or value)	Mean	Variance	Distribution
PROSPECT	C _{ar} (carotenoid content, µg/cm ²)	12	-	-	-
	C _w (equivalent water thickness, cm)	0.01	-	-	-
	C _{brown} (brown pigment content)	0	-	-	-
	C _m (dry matter content, g/cm ²)	0.001–0.01	0.005	0.005	Gauss
	C _{ab} (leaf chlorophyll a + b Concentration, µg/cm ²)	10–80	40	20	Gauss
	N (leaf structure parameter)	1–1.8	1.4	0.5	Gauss
SAIL	LAI (leaf area index)	0–8	2	3	Gauss
	ALA (average leaf angle inclination)	40–70	55	10	Gauss
	SZA (solar zenith angle)	35	-	-	-
	Hot (hot-spot parameter)	0.1–0.5	0.2	0.5	Gauss

2.4. Sensitivity analysis methods

Global sensitivity analysis (SA) methods have been widely applied in remote sensing. Compared with local SA algorithms, global SA methods search the full range of parameter variations instead of merely a local area around a mean value (Bowyer and Danson, 2004). In this study, the Extended Fourier Amplitude Sensitivity Test (EFAST) is used to quantify the sensitivities of the variables (seven bands) to the LAI and LCC variations. Based on the variances of the simulated results caused by different input parameters, EFAST assesses the importance of each parameter and their influences on the simulated results. EFAST allows for the calculation of the first-order (S_i) and total effect (S_{Ti}) sensitivity indices. The S_i index represents the main effect contribution of input variables. The S_{Ti} index is an overall measurement of the first-order effect and higher-order effects due to the interactions among all

parameters (Vazquez-Cruz et al., 2014). S_i and S_{Ti} indices are calculated as follows:

$$S_i = \frac{V_i}{V(Y)}, \quad V(Y) = \sum_i V_i + \sum_{i \neq j} V_{ij} + \sum_{i \neq j \neq m} V_{ijm} + \dots + \sum_{i \neq j \neq \dots \neq k} V_{ij\dots k} \quad (1)$$

$$V_i = V[E(Y/x_i)] \quad (2)$$

$$V_{ij} = V[E(Y/x_i, x_j)] - V_i - V_j \quad (3)$$

$$S_{Ti} = (V_i + V_{ij} + \dots + V_{ij\dots k})/V(Y) \quad (4)$$

where V(Y) is the total variance of model simulated result (Y) caused by the change of parameter (X) within the value range; V_i represents the variance of parameter x_i; E(Y/x_i) is the conditional expectation of Y to x_i; E(Y/x_i, x_j) is the conditional expectation of Y to x_i and x_j; V_{ij} is the variance of interaction between parameter x_i and x_j; V_{ij...k} is the variance of interaction between parameter x_i, x_j, ..., x_k.

2.5. VIs for LAI and LCC estimation

Five two-bands VIs forms (e.g., NDVI_{a,b}, MSR_{a,b}, CI_{a,b}, OSAVI_{a,b} and EVI_{2a,b}) were used for LAI and LCC estimation (Table 4). In those forms, a and b refer to different band reflectances of S2. To determine the best VIs for LAI and LCC estimation, several “a,b” combinations were compared in this study. Optimal a and b were determined based on the global sensitivity analysis result. In addition to those two-bands VIs, six three-bands VIs were also investigated for LCC estimation since accurate LCC estimations were more difficult to achieve. Among those six VIs, the triangular chlorophyll index (TCI), moderate-resolution imaging

Table 4
VIs used for LAI and LCC estimation.

Index	Formula	Application	Reference
NDVI _{a,b} (Normalized difference vegetation index)	(R _a -R _b)/(R _a + R _b)	Used for LAI and LCC	(Rouse et al., 1974)
MSR _{a,b} (Modified simple ratio)	[(R _a /R _b)-1]/[(R _a /R _b) + 1] ^{0.5}	Used for LAI and LCC	(Chen, 1996)
CI _{a,b} (Chlorophyll index)	(R _a -R _b)/R _b	Used for LAI and LCC	(Gitelson et al., 2003)
OSAVI _{a,b} (Soil-adjusted vegetation index)	1.16 × (R _a -R _b)/(R _a + R _b + 0.16)	Used for LAI and LCC	(Rondeaux et al., 1996)
EVI _{2a,b} (Two-band enhanced vegetation index)	2.5 × (R _a - R _b)/(R _a + 2.4 × R _b + 1)	Used for LAI and LCC	(Jiang et al., 2008)
TCI (The triangular chlorophyll index)	1.2 × (R _{RE1} -R _{Green})-1.5 × (R _{Red} -R _{Green}) × (R _{RE1} /R _{Red}) ^{0.5}	Used for LCC	(Broge & Leblanc, 2001)
MTCI (Moderate-resolution imaging spectrometer terrestrial chlorophyll index)	(R _{RE3} -R _{RE2})/(R _{RE2} -R _{Green})	Used for LCC	(Dash and Curran, 2007)
DCNI (Double-peak canopy nitrogen index)	[(R _{RE1} -R _{Green} + 0.09) × (R _{RE1} -R _{Red})]/(R _{RE2} -R _{Green})	Used for LCC	(Jin et al., 2014)
TVI (Triangular vegetation index)	0.5 × [120 × (R _{NIR1} -R _{Green})-200 × (R _{Red} -R _{Green})];	Used for LCC	(Broge & Leblanc, 2001)
TCARI/OSAVI (Transformed chlorophyll absorption in the reflectance index/optimized soil-adjusted vegetation index)	3 × [(R _{RE1} - R _{Red}) - 0.2 × (R _{RE1} -R _{Green}) × (R _{RE1} /R _{Red})]/[1.16 × (R _{NIR1} - R _{Red})/(R _{NIR1} + R _{Red} + 0.16)]	Used for LCC	(Rondeaux et al., 1996)
RECAI (Red-edge-chlorophyll absorption index)	(R _{NIR1} - R _{RE2})/[R _{Green} × (R _{RE1} /R _{Green})]	Used for LCC	(Cui et al., 2019)

Notes: a and b refer to the seven bands of Sentinel-2 used in this study.

spectrometer terrestrial chlorophyll index (MTVI), and red-edge-chlorophyll absorption index (RECAI) were developed for LCC estimation based on the absorption and reflection characteristics of chlorophyll. The double-peak canopy nitrogen index (DCNI) was developed for leaf nitrogen estimation at first (Jin et al., 2014), but also achieved good performance in LCC estimation in many studies due to chlorophyll content being highly related to nitrogen (Jay et al., 2017). The triangular vegetation index (TVI), proposed by Broge and Leblanc (2001), assumed that the decrease of red band reflectance and the increase of NIR band reflectance would change the total area of a triangle. Due to its high correlation with chlorophyll absorption, TVI was considered as one commonly used variable for LCC estimation (Cui et al., 2019). By providing a canopy chlorophyll measurement and then correcting for biomass, the ratio of transformed chlorophyll absorption in the reflectance index (TCARI) and optimized soil-adjusted vegetation index (OSAVI) had been regarded as the traditional leaf chlorophyll indices in many studies (Berger et al., 2020). Therefore, these three VIs were appropriately selected for this study and their corresponding equations were listed in Table 4.

2.6. Random forest regression

Random forest regression (RFR), first proposed by Breiman in 2001 (Breiman, 2001), has become one of the most popular machine learning algorithms in many research fields. To achieve accurate predictions, the RFR integrates the results from a large number of decision trees generated by the algorithm. RFR not only achieves accurate and stable predictions, but also shows high efficiency in processing high-dimensional data. In this study, several VIs shown in Table 3 are used as inputs in the RFR algorithm for LAI and LCC estimation. The number of decision trees in the forest (n) and the number of input variables chosen at each split (m) are two important parameters that may influence the calculation speed and accuracy of the RFR algorithm. In this study, m was set to 1/3, and n was set to 500 based on several trial runs.

2.7. Basic LAI estimation model construction and LCC estimation

Before introducing LCC information, the basic LAI estimation model needs to be determined (see Fig. 3). First, the LAI-sensitive bands are selected based on a global sensitivity analysis. Then, only the LAI-sensitive bands can be adopted as “ a ” and “ b ” to construct LAI-

sensitive VIs, as shown in Table 4. To be consistent with earlier studies of VIs construction (Chen, 1996; Gitelson et al., 2003), the central wavelength of “ a ” is smaller than that of “ b ”. Moreover, “ a ” and “ b ” should not both belong to the NIR region. Every five VIs (e.g., $NDVI_{a,b}$, $MSR_{a,b}$, $CI_{a,b}$, $OSAVI_{a,b}$, $EVI2_{a,b}$) calculated by the same bands are considered as a group of inputs for LAI estimation using the RFR algorithm. As a result, each group of inputs (or every band combination) generates one LAI estimation model. To make full use of the canopy reflectance information, this study applied two groups of inputs for the LAI estimation. According to the previous studies about the description and definition of LAI saturation (Delegido et al., 2013; Xie et al., 2018), the evaluations of LAI estimation models were divided into two parts: $LAI \leq 3$ (low LAI value range) and $LAI > 3$ (moderate-to-high LAI value range). In each part, models with root mean square error (RMSE) values smaller than (or equal to) 1.0 were selected. As shown in Fig. 3, subset 1 contains models with $RMSE \leq 1$ in the low LAI value regions while subset 2 contains models with $RMSE \leq 1$ in the moderate-to-high LAI value regions. Each model has a corresponding group of inputs. Then, a number of new models whose inputs were consisted of two groups of VIs (one group used by the model from Subset 1 and one group used by the model from Subset 2) were developed for LAI estimation. Finally, the model with the best performance was selected as the basic LAI estimation model.

Eleven VIs were used for LCC estimation (see Table 4). Other than six three-band VIs, the construction of the remaining five two-band VIs was also based on the global sensitivity analysis. The best combinations of “ a ” and “ b ” were determined by the performance of LCC estimation model.

2.8. LAI estimation model involving LCC information

After constructing the basic LAI estimation model, the LCC simulations, described as the pure LCC, is used as an additional variable to develop the LAI estimation model (Fig. 4). This “pure LCC” is estimated using LCC-sensitive VIs. However, it is widely known that estimation of LCC is more complicated than LAI. Therefore, adding estimated LCC with large errors to LAI estimation may cause lower accuracy improvements or even unexpected accuracy decrease. Therefore, this study proposed two modified methods for introducing the LCC to achieve higher LAI estimation accuracy.

Modified method 1: The noise-adding LCC (noisy LCC) data are used

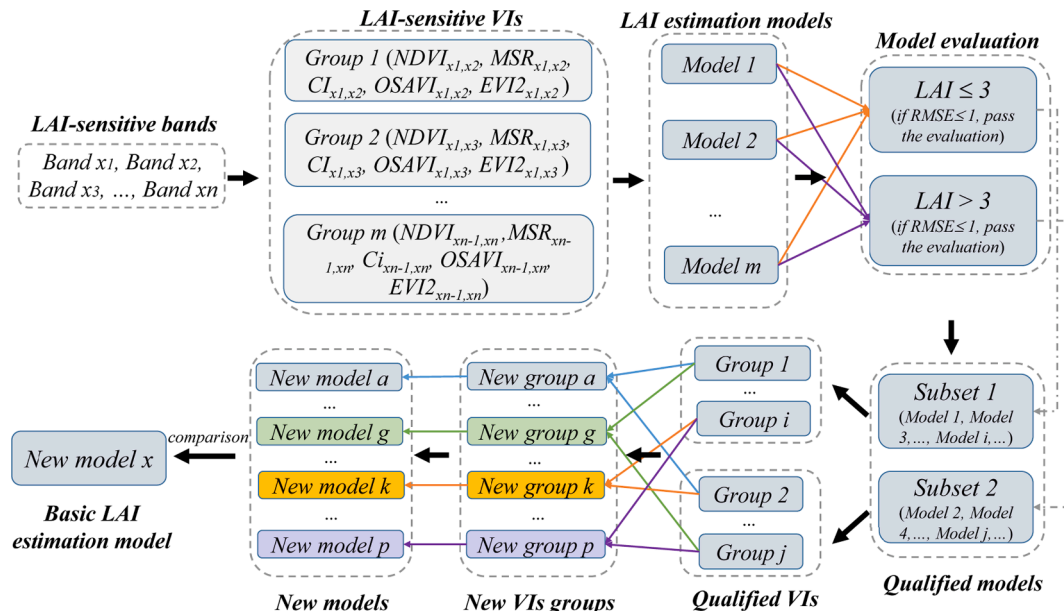


Fig. 3. Process of basic LAI estimation model generation.

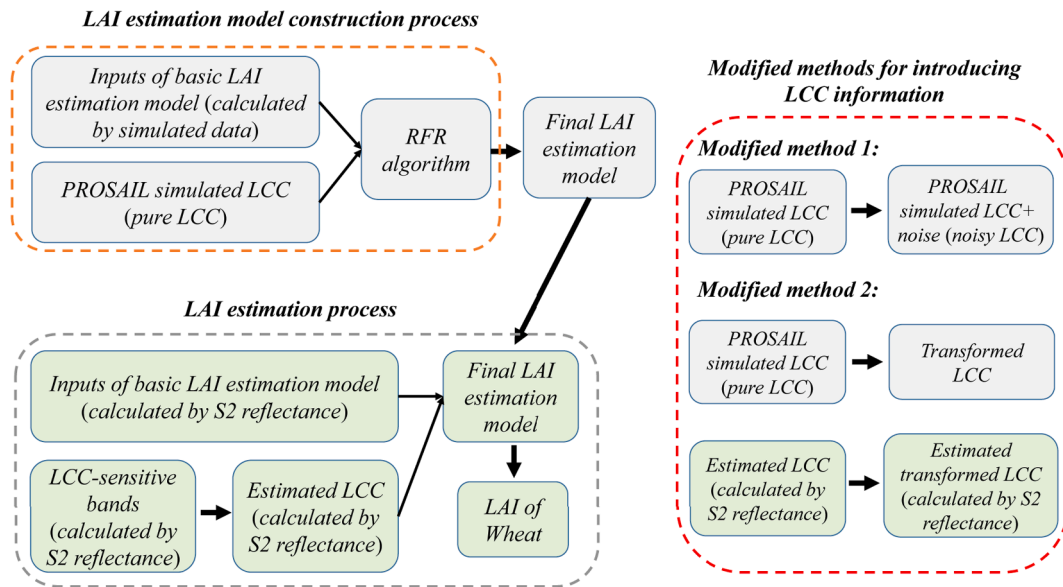


Fig. 4. Process of final LAI estimation model generation using the pure LCC, noisy LCC and transformed LCC.

instead of pure LCC data, which is defined as $F_1(\text{LCC})$ (see Eq. (5)). This modification aims to improve the performance by adding an appropriate amount of noise into the pure LCC data. Thus, the difference between LCC information used in the theoretical model and in the field validation can be reduced.

$$\begin{cases} F_1(\text{LCC}) = \text{LCC} + a_1 \\ a_1 = x\% \times 0.5 \times (\max(\text{LCC}) + \min(\text{LCC})) \\ x \in [5, 100], \text{step} = 5, \max(\text{LCC}) = 80, \min(\text{LCC}) = 10 \end{cases} \quad (5)$$

where the LCC represents the pure LCC values and a_1 represents the LCC noise. a_1 is set to the times of 45 which is the average value of simulated LCC maximum value ($80 \mu\text{g}/\text{cm}^2$) and minimum value ($10 \mu\text{g}/\text{cm}^2$). To find the best noise increment, $x\%$ is set in a range of 5% to 100% with the step of 5%.

Modified method 2: The functional equation of LCC (transformed LCC) instead of pure LCC is used (see Fig. 4). Similar to LAI, the LCC also suffer from underestimation due to the saturation of red band (Clevers and Gitelson, 2013), which may cause accuracy LAI estimation accuracy decrease. Three transformed LCC ($F_2(\text{LCC})$: power function, $F_3(\text{LCC})$: logarithmic function, and $F_4(\text{LCC})$: growth equation) are proposed to reduce the error caused by LCC underestimation (see Equations (6) to (8)). In $F_4(\text{LCC})$, the LCC values are divided by 10 to increase the difference between the maximum and minimum values. All of these transformations exhibit slow uptrends in the moderate-to-high LAI regions, which can mitigate the underestimation phenomenon by decreasing the differences in the LCC. Finally, the transformation equation with the greatest LAI estimation accuracy improvement is selected as the best method to introduce the LCC information.

$$F_2(\text{LCC}) = \text{LCC}^{0.5} \quad (6)$$

$$F_3(\text{LCC}) = \log(\text{LCC}) \quad (7)$$

$$F_4(\text{LCC}) = 1 - e^{-(\text{LCC}/10)} \quad (8)$$

2.9. Accuracy assessment

Two kinds of validations are used in this study including the theoretical validation to test the model fitness, and the field-based validation to test the model practicability in the actual field. For theoretical validation, 100,000 simulations are randomly selected among the 150,000 samples, and the remaining 50,000 samples are used as the validation

set. In the field-based validation, 218 field LAI measurements are used to assess the LAI estimation accuracy. RMSE is selected as the indicator to evaluate both theoretical and practical performance of LAI estimations.

3. Results

3.1. EFAST sensitivity analysis

The S_i and S_{T_i} values representing the contributions of LAI and LCC to the reflectances are presented in Fig. 5. These two indices show the similar results regarding the sensitivity of each band. The reflectances of green and RE1 bands are more sensitive to the LCC, while the reflectance of RE2, RE3, NIR1, and NIR2 bands are significantly sensitive to LAI. The sum of S_i values of LAI and LCC in the red band is 0.915, which indicates 91.5% of the simulated red band canopy reflectance can be explained by LAI and LCC. Compared with other bands (RE2, RE3, NIR1, and NIR2), the S_i and S_{T_i} values of LCC in Red band are >0.2 . This result demonstrates that although red band can be used for LAI estimation, the influence of LCC is also nonnegligible. Therefore, the LAI sensitive bands are red, RE2, RE3, NIR1 and NIR2. Since red band is also influenced by the LCC, the determined LCC sensitive bands are green, red and RE1.

3.2. LAI estimation accuracies based on different VIs

According to the EFAST analysis and the VIs construction criterion, nine groups of VIs were investigated to generate LAI estimation models (M1 ~ M9 in Table 5), and their performances were shown in Fig. 6. Although using the RE2-based VIs improved the estimation accuracies in the moderate-to-high LAI region, they also caused overestimation in the low LAI region (see M2, M5, M8 in Fig. 6). Conversely, the use of red-based VIs achieved higher estimation accuracies in the low LAI region, while it caused underestimation in the moderate-to-high LAI region (see M1, M4, M7 in Fig. 6). Therefore, using the five VIs that only contain the information from two bands could hardly achieve satisfactory performance during the whole growing season.

As shown in Table 6, four models (Subset 1: M1, M4, M7, M9) are appropriate for low region LAI estimation while three models (Subset 2: M2, M5, M8) are suitable for moderate-to-high region LAI estimation. Therefore, to improve LAI estimation accuracy over the entire growing season, two VIs groups containing ten variables are used in the RFR algorithm for LAI estimation (Table 7). Adding more VIs that contrasted with the other bands have significantly improved the LAI estimation

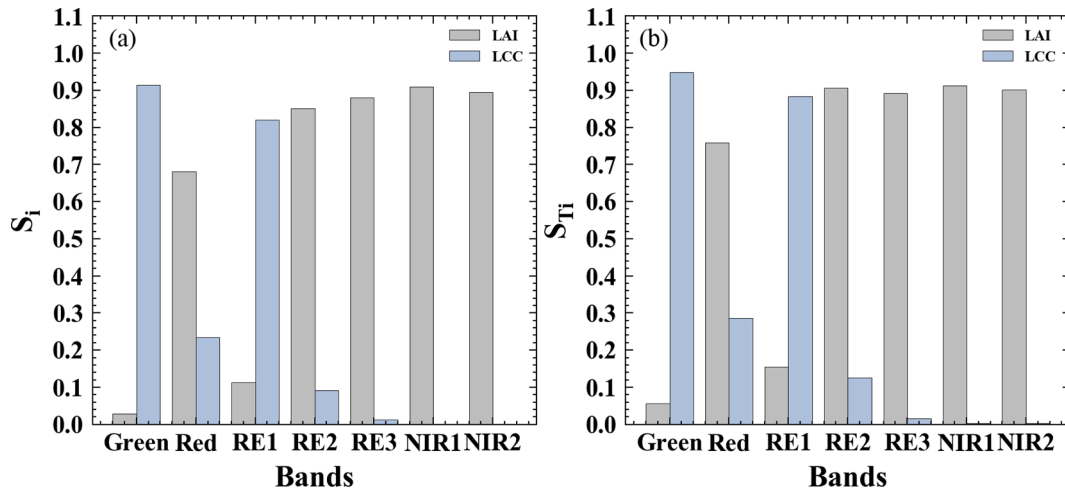


Fig. 5. (a) First-order (S_i) and (b) total effect (S_{Ti}) sensitivity analysis results of the LAI and LCC on the simulated S2 MSI band reflectance.

Table 5

Descriptions of the nine LAI estimation models.

Model	Description (input variables)
M1	NDVI _{NIR2,Red} , MSR _{NIR2,Red} , CI _{NIR2,Red} , OSAVI _{NIR2,Red} , EVI _{NIR2,Red}
M2	NDVI _{NIR2,RE2} , MSR _{NIR2,RE2} , CI _{NIR2,RE2} , OSAVI _{NIR2,RE2} , EVI _{NIR2,RE2}
M3	NDVI _{NIR2,RE3} , MSR _{NIR2,RE3} , CI _{NIR2,RE3} , OSAVI _{NIR2,RE3} , EVI _{NIR2,RE3}
M4	NDVI _{NIR1,Red} , MSR _{NIR1,Red} , CI _{NIR1,Red} , OSAVI _{NIR1,Red} , EVI _{NIR1,Red}
M5	NDVI _{NIR1,RE2} , MSR _{NIR1,RE2} , CI _{NIR1,RE2} , OSAVI _{NIR1,RE2} , EVI _{NIR1,RE2}
M6	NDVI _{NIR1,RE3} , MSR _{NIR1,RE3} , CI _{NIR1,RE3} , OSAVI _{NIR1,RE3} , EVI _{NIR1,RE3}
M7	NDVI _{RE3,Red} , MSR _{RE3,Red} , CI _{RE3,Red} , OSAVI _{RE3,Red} , EVI _{RE3,Red}
M8	NDVI _{RE3,RE2} , MSR _{RE3,RE2} , CI _{RE3,RE2} , OSAVI _{RE3,RE2} , EVI _{RE3,RE2}
M9	NDVI _{RE2,Red} , MSR _{RE2,Red} , CI _{RE2,Red} , OSAVI _{RE2,Red} , EVI _{RE2,Red}

accuracies (Fig. 7). As shown in Fig. 8, all of the new models achieved LAI estimations with RMSE ≤ 1.0 in two LAI regions (LAI ≤ 3 and LAI > 3). Therefore, merging the variables that are suitable for different growth stages can generate accurate LAI estimates during the whole growing period. Compared to using variables of M2 and M5, the adoption of M8 variables (NDVI_{RE3,RE2}, MSR_{RE3,RE2}, CI_{RE3,RE2}, OSAVI_{RE3,RE2}, EVI_{RE3,RE2}) resulted in smaller accuracy improvements (see NM3, NM6, NM9, NM12, in Figs. 7 and 8). According to Table 6, M8 not only provides LAI estimates with lower RMSE value in the moderate-to-high LAI region, but also provides significant LAI overestimation (RMSE = 1.970) at low LAI region. Although the addition of other VIs has effectively weakened the overestimation, the M8-based models (NM3, NM6, NM9, and NM12) still show lower LAI estimation accuracies with RMSE values ranging from 0.860 to 1.203 in the low LAI region. Among those twelve new LAI estimation models, NM5 achieves the best performance (RMSE = 0.832) and is selected as the basic LAI estimation model.

3.3. Final LAI estimation model containing LCC information

The LCC information was estimated and added to the basic LAI estimation model as one of the inputs to explore its contribution to the improvements of LAI estimation accuracies. Three different methods to introduce LCC information (pure LCC, noisy LCC, and transformed LCC) were compared.

3.3.1. Theoretical validation based on simulated data

By adding the pure LCC values, the LAI estimation performance was improved significantly (with RMSE decreasing by 21.55% (Fig. 9)). Moreover, according to the two fitting lines (Fig. 9), the addition of LCC information reduced the bias in both the low and moderate-to-high LAI regions. Therefore, the theoretical validation results suggested the effectiveness of LCC for improving LAI estimation.

3.3.2. Selecting best VIs for LCC estimation

Five two-bands VIs (NDVI_{a,b}, MSR_{a,b}, CI_{a,b}, OSAVI_{a,b}, and EVI_{a,b}) and six three-bands VIs (TCI, MTCl, DCNI, TVI, TCARI/OSAVI, and RECAI) were both tested for LCC estimation. According to the EFAST sensitivity results, three LCC estimation models that use different groups of VIs were developed (see Table 8). M2_{LCC} shown the highest LCC estimation accuracy, which also indicated that the combination of RE1 and red bands could generate better LCC estimation.

3.3.3. LAI estimation using different LCC introducing methods

After integrating the pure LCC values into LAI estimation model, the RMSE decreased by 4.09% (Fig. 10b). The distributions of the scattered points were closer to the 1:1 line compared to the basic LAI estimation model (Fig. 10a), especially in low LAI region. However, compared with the performances of theoretical validation shown in Fig. 9, the LAI estimation accuracy improvement attributed to adding pure LCC was not significant.

In the theoretical verification (see Fig. 11), adding noise with $x\%$ equal to 100% (or noise values ranging from -45 to 45) increased RMSE by 0.113 compared with the results shown in Fig. 9b. Based on field measurements validation, adding noise at level of 5% to 50% to the simulated LCC data slightly improved LAI estimation accuracies. With increasing amounts of LCC noise, the LAI estimation accuracies increased steadily when x ranged from 5 to 25, whereas the LAI estimation accuracies decreased when x range from 30 to 100. The highest LAI estimation accuracy was achieved (RMSE = 0.781) when x equals to 25 (Fig. 12a). According to the two-part-LAI-evaluation, this model achieved LAI estimation performances with RMSE of 0.713 in the low LAI region and RMSE of 0.839 in the moderate-to-high LAI region.

For adding the transformed LCC to the LAI estimation model, using the power function transformation (F_2), logarithmic function (F_3) and growth Equation (F_4) decreased the RMSE values by 5.29%, 7.45%, and 11.54% compared with the basic LAI estimation model, respectively (see Table 9). Furthermore, F_4 achieved the highest LAI estimation accuracy with RMSE of 0.736 (Fig. 12b). In addition, this model achieved LAI estimation performances with RMSE value of 0.646 and 0.810 in the low LAI region and moderate-to-high LAI region, respectively.

To demonstrate the importance of the methods used to integrate additional band information, this study also tested the performances of ten LAI-sensitive VIs and six bands (green, red, RE1, RE2, RE3, and NIR1) used in LCC estimation to construct the LAI estimation model (Fig. 12c). The results shown that direct adding additional band reflectance data as inputs caused a significant LAI estimation accuracy decrease (RMSE = 0.875). In addition, compared with the basic LAI estimation model (Fig. 10a), using ten VIs and six bands reflectances

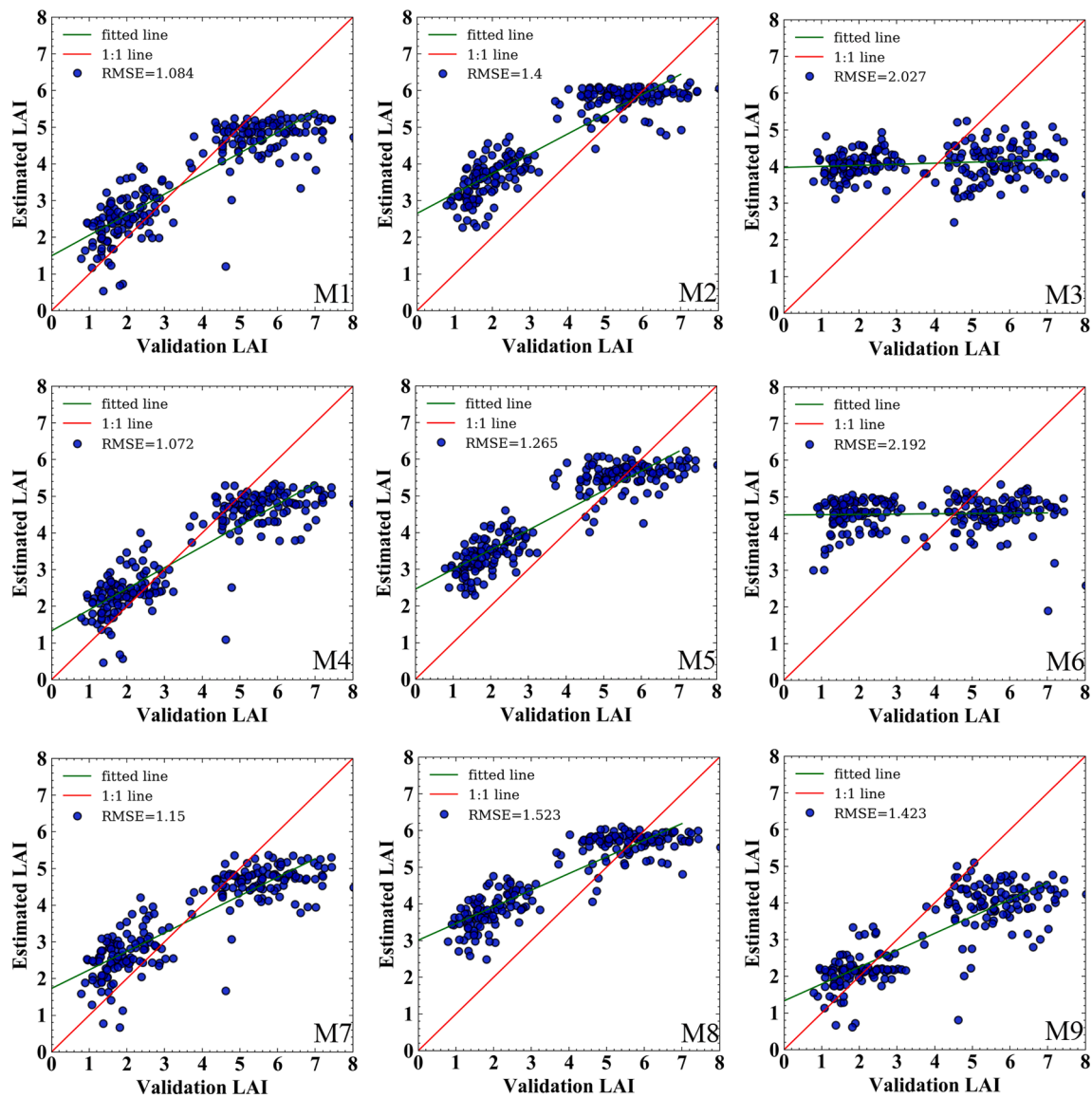


Fig. 6. Performances of the nine LAI estimation models based on different VIs.

Table 6
RMSE values of different LAI estimation models from subset 1 and subset 2.

Subsets	Models	RMSE	
		LAI ≤ 3	LAI > 3
Subset 1	M1	0.890	1.302
	M4	0.750	1.332
	M7	0.923	1.361
	M9	0.641	1.916
Subset 2	M2	1.767	0.905
	M5	1.593	0.827
	M8	1.970	0.874

produced larger RMSE values of 0.754 and 0.986 in the low and moderate-to-high LAI region.

4. Discussion

Accurate LAI estimation based on medium-resolution multispectral data is always a challenging task in quantitative remote sensing. Many studies have confirmed that saturation occurs at moderate-to-high LAI region when using traditional combined Red-NIR VIs (Sinha et al.,

Table 7
Descriptions of the twelve new LAI estimation models.

Model	Description (input variables)	Model	Description (input variables)
NM1	Variables of M1 and M2	NM2	Variables of M1 and M5
NM3	Variables of M1 and M8	NM4	Variables of M4 and M2
NM5	Variables of M4 and M5	NM6	Variables of M4 and M8
NM7	Variables of M7 and M2	NM8	Variables of M7 and M5
NM9	Variables of M7 and M8	NM10	Variables of M9 and M2
NM11	Variables of M9 and M5	NM12	Variables of M9 and M8

2020). To solve this problem, RE bands that are more sensitive to LAI are widely applied to replace red band. However, some studies have indicated that the RE bands are also influenced by LCC, which is a factor that cannot be ignored with respect to the errors in LAI estimation (Xie et al., 2018). Therefore, a novel LAI estimation method involving LCC information was proposed in the model. Instead of excluding LCC-sensitive band reflectance data in LAI estimation model, this method used both LAI-sensitive VIs and LCC information. By using the complex nonlinear relationship between LAI and LCC information, the canopy reflectance has been incorporated efficiently, and the LAI estimation accuracies had been significantly improved.

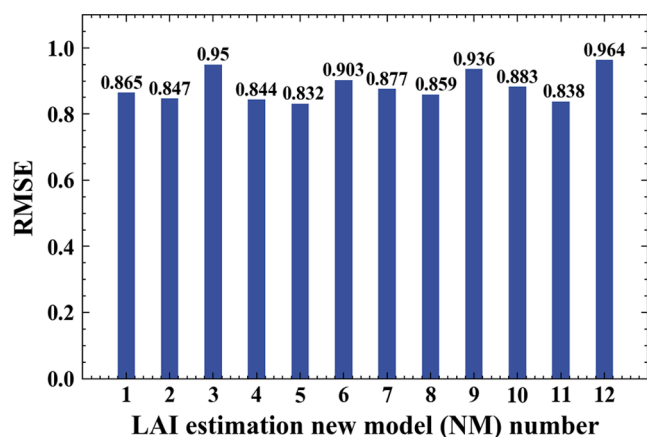


Fig. 7. Performances of the twelve new LAI estimation models.

To reduce the LCC effect in the first step, a basic LAI estimation model was developed by using only LAI-sensitive VIs. The EFAST analysis demonstrated that LCC contributed to the changes of visible and red-edge band reflectances, whereas LAI particularly influenced the reflectances in red, RE and NIR bands (Xie et al., 2018; Berger et al., 2020). The results also shown that LCC clearly influenced the reflectances of green and RE1 bands. This was because the red band, which was affected by chlorophyll content, experienced displacement in the red-edge domain when it was saturated at high LCC values. These results were similar to previous studies which indicated that the 550 nm and 750 nm bands were suitable for LCC estimation (Sims and Gamon, 2002). In addition, the results also indicated that the reflectances of red,

RE2, RE3 and other two NIR bands were mostly influenced by LAI, which was also consistent with the previous study (Sun et al., 2020). Furthermore, LAI-sensitive VIs were used to test their capabilities in LAI estimation. However, one group of VIs only containing information of two LAI sensitive band reflectances, which was inadequate for accurate LAI estimation (see Fig. 6). As shown in Fig. 6, the use of five RE2-based VIs effectively mitigated the underestimation in the moderate-to-high LAI region, but caused overestimation in the low LAI region. Previous studies had suggested that RE-based VIs could improve LAI estimation accuracies when applied to crops with consistent chlorophyll content, such as for one growth stage (Delegido et al., 2013). However, the RE2-based VIs shown a limited capability for improving the LAI estimation accuracies throughout the entire growing period in this study. To overcome this problem, two groups of VIs with good performances in different LAI regions were used as develop the basic LAI estimation model, and the model contained information from the red, RE2, and NIR1 bands, achieved the highest LAI estimation accuracy. This agreed with the study of Xie et al (Xie et al., 2018), which indicated that combining red and RE band reflectances could weaken the underestimation and overestimation phenomenon in LAI estimation.

Table 8 Performances of the three LCC estimation models in theoretical validation.

Models	RMSE
M1 _{LCC} (Inputs: NDVI _{RE1,Green} , MSR _{RE1,Green} , CI _{RE1,Green} , OSAVI _{RE1,Green} , EVI _{RE1,Green} , TCI, MTCl, DCNI, TVI, TCARI/OSAVI)	15.058
M2 _{LCC} (Inputs: NDVI _{RE1,Red} , MSR _{RE1,Red} , CI _{RE1,Red} , OSAVI _{RE1,Red} , EVI _{RE1,Red} , TCI, MTCl, DCNI, TVI, TCARI/OSAVI)	9.629
M3 _{LCC} (Inputs: NDVI _{Red,Green} , MSR _{Red,Green} , CI _{Red,Green} , OSAVI _{Red,Green} , EVI _{Red,Green} , TCI, MTCl, DCNI, TVI, TCARI/OSAVI)	11.583

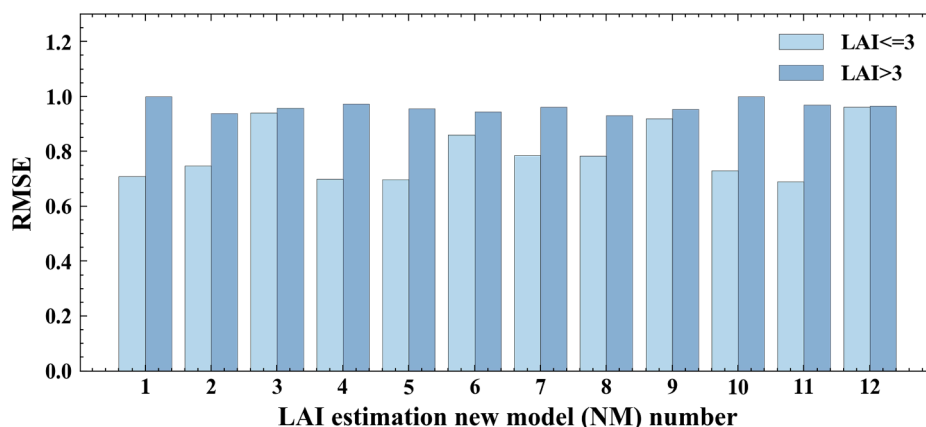


Fig. 8. RMSE values of the twelve new LAI estimation models.

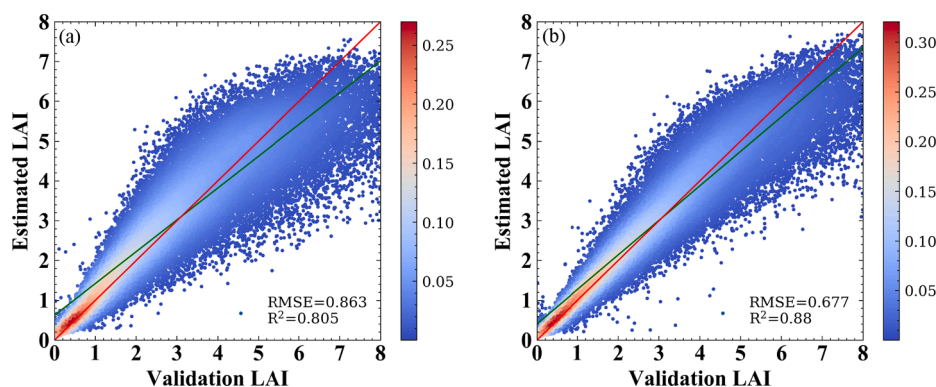


Fig. 9. Theoretical validation results of the LAI estimation model using LAI-sensitive VIs (a) and using LAI-sensitive VIs and simulated LCC (b).

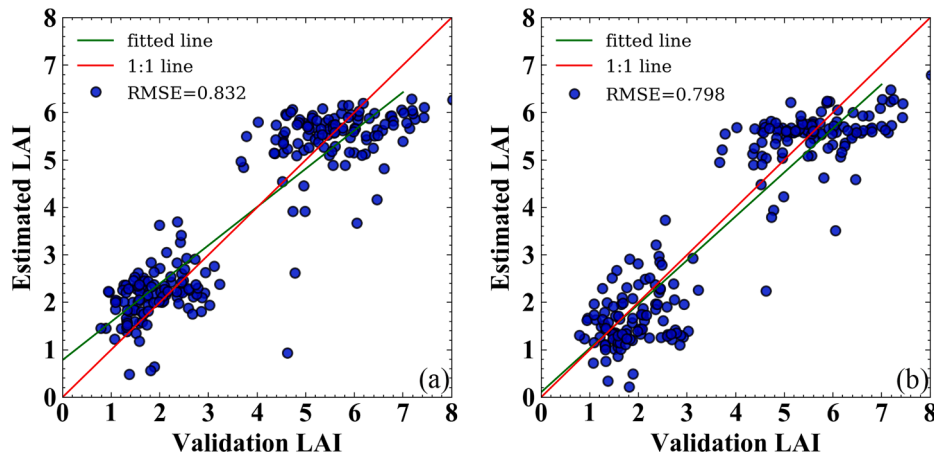


Fig. 10. Model performance of the basic LAI estimation model (a) and using LAI-sensitive VIs and pure LCC (b).

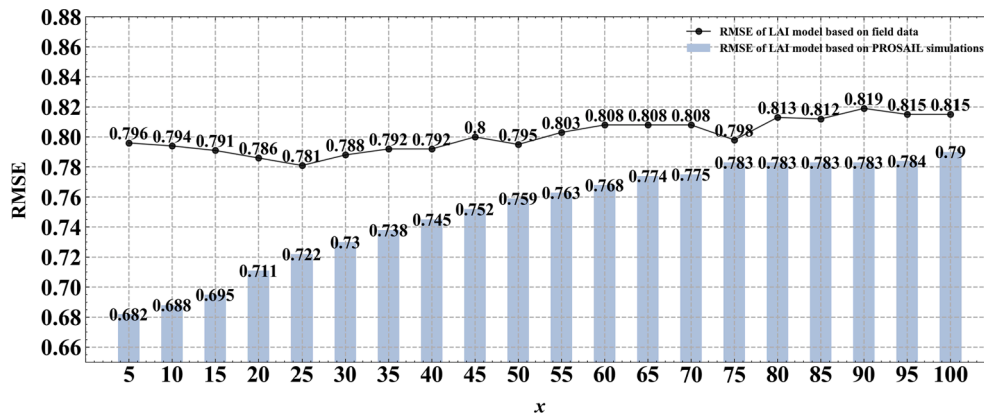


Fig. 11. RMSE values of the LAI estimation models using VIs and noisy LCC data.

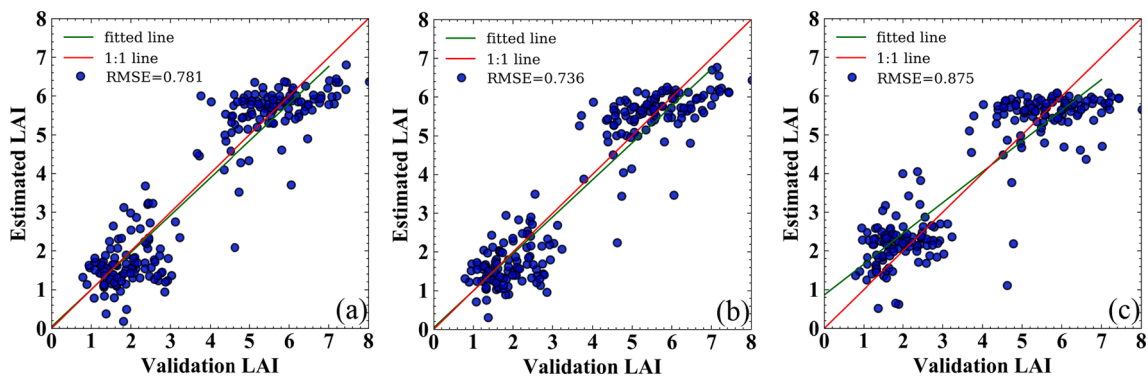


Fig. 12. Model performances using different inputs: the noisy LCC (a), the F_4 transformed LCC (b), and ten LAI-sensitive VIs and six band reflectances (green, red, RE1, RE2, RE3 and NIR1) (c). (For interpretation of the references to colour in this figure legend, the reader is referred to the web version of this article.)

Table 9

Field measurement verification of LAI estimation after adding transformed LCC.

Model formation	RMSE
F_2 (LCC) = $LCC^{0.5}$	0.788
F_3 (LCC) = $\log(LCC)$	0.770
F_4 (LCC) = $1 - e^{-LCC/10}$	0.736

In previous LAI estimation studies based on VIs, only information from a few sensitive bands was used. Some researchers suggested that although the rest of the bands were not recommended for constructing modified VIs, they could be useful when combining with VIs to increase the information regarding canopy status (Dong et al., 2020). However, the introducing methods of additional bands or VIs for LAI estimation were very important. As shown in Fig. 12c, adding additional bands directly to construct the LAI estimation model resulted significant accuracy decrease. This was because the reflectances of green and RE1 band were more sensitive to LCC than to LAI. When adding these bands to the LAI estimation models, the LCC caused reflectance changes were

mistakenly considered to be resulted from LAI. For example, as a catalyst for plant photosynthesis, the chlorophyll contents promoted plant growth in the early growing stage, including height and total leaf area increase. In the maturation stage, the leaf areas and chlorophyll contents decreased as the bottom leaves turned yellow and fell off. Therefore, the correlation between these two parameters was subtle and complex. Fortunately, the RFR algorithm used in this study successfully mapped the relationship between them (see Fig. 9), and LCC ranked fourth among the importance of 11 inputs. When compared with other studies, this approach not only reduced the LCC effect by developing a basic LAI estimation model, but also made full use of the canopy reflectance by including the nonlinear correlation between LCC and LAI in the final model. The LAI estimation accuracies were improved by the machine learning regression algorithm twice (one for LCC estimation and the other for LAI estimation). Therefore, the LCC information used in this study could also be regarded as a complex VI that integrated the information from multiple bands. Moreover, since the LCC values were generated by the PROSAIL simulation, this approach was independent of field LCC measurements.

This study discussed the effects of three different LCC introducing methods (pure LCC, noisy LCC, and transformed LCC). By adding pure LCC, the LAI estimation accuracy had been improved with RMSE reduced by 4.08%. However, in contrast to the theoretical verification, the accuracy improvement in the field-based verification (Fig. 10b) was not significant. The first reason might be the LCC estimation error. Previous studies have shown that the Sen2Cor atmospheric correction algorithm produced an amount of noise between 5% and 10% (Brede et al., 2020). Therefore, using the pure LCC data to generate a LAI estimation model would cause lower accuracy improvement, while using the noisy LCC data had successfully improved the LAI estimation accuracy of the field-based verification. This was because the noise added to the pure LCC data decreased the importance of LCC among all variables. The second reason might be that the LCC estimation also suffered from saturation effect in moderate-to-high value region (Cui et al., 2019). Adding the pure LCC value improved the LAI estimation accuracy mostly in the low LAI region. Therefore, the LCC information only functioned effectively when it was estimated accurately. In previous studies, the use of transformations or combinations of variables instead of the original values was an effective means for accuracy improvements (Chen, 1996; Delegido et al., 2013). The core concept of those changes was to reduce some inevitable influences. Based on this conception, three transformations (power function, logarithmic function, and growth equation) were applied to decrease the differences between the actual and estimated LCC information in the high value region. Using the growth equation of LCC achieved the highest LAI estimation accuracy, which improved LAI estimation accuracy with RMSE reduced by 11.54% compared with NM5. In general, both LCC introducing methods improved LAI estimation accuracy. However, they had varying improvements since the two modifications were focused on solving different problems. In contrast to the first modification, the second modification achieves better LAI estimates especially in the low LAI region. This indicated that the second modification not only reduced the saturation effect of LCC, but also has a better correlation with LAI in the low LAI region. While in the first modification, the noise was added to all data. Larger noise had a better effect on the moderate-to-high LAI region, but it also increased the RMSE value in the low LAI region.

5. Conclusions

This study proposed a novel approach to improve LAI estimation accuracy by involving LCC information in the model. The main conclusions are as follows:

- (1) In the basic LAI estimation model, the use of RE2-based VIs and red-based VIs can achieve better LAI estimations for the entire growth period. In addition, the RE2-based VIs can achieve higher

LAI estimation accuracies when $LAI > 3$, but they also caused overestimation when $LAI \leq 3$.

- (2) The addition of pure LCC can improve LAI estimation accuracy, but it is more effective in low LAI region ($LAI \leq 3$). Adding noisy LCC and transformed LCC can both improve the LAI estimation accuracy for both growth periods.

Compared with the traditional LAI-sensitive-VIs-based method, involving LCC information is more reasonable for taking more canopy information into consideration and better reflects the seasonal characteristics of wheat. Further studies will be focus on investigating this method for different vegetation types, and more field measurements from different growth phases for validation.

CRedit authorship contribution statement

Zhulin Chen: Conceptualization, Methodology, Software, Validation, Writing – original draft, Writing – review & editing, Formal analysis. **Kun Jia:** Conceptualization, Methodology, Writing – review & editing, Resources, Funding acquisition. **Xiangqin Wei:** Methodology, Writing – review & editing, Validation, Supervision. **Yan Liu:** Investigation, Writing – review & editing. **Yulin Zhan:** Investigation, Writing – review & editing. **Mu Xia:** Investigation, Writing – review & editing. **Yunjun Yao:** Investigation, Writing – review & editing. **Xiaotong Zhang:** Investigation, Writing – review & editing.

Declaration of Competing Interest

The authors declare that they have no known competing financial interests or personal relationships that could have appeared to influence the work reported in this paper.

Acknowledgments

This research was funded by the National Key R&D Program of China (2020YFE0200700), the National Natural Science Foundation of China (42171318), the Major Special Project - the China High-Resolution Earth Observation System (30-Y30F06-9003-20/22), and the Tang Scholar Program (K. Jia is a Tang Scholar of Beijing Normal University).

References

- Berger, K., Verrelst, J., Féret, J.-B., Wang, Z., Wocher, M., Strathmann, M., Danner, M., Mauser, W., Hank, T., 2020. Crop nitrogen monitoring: Recent progress and principal developments in the context of imaging spectroscopy missions. *Remote Sens. Environ.* 242, 111758.
- Bowyer, P., Danson, F.M., 2004. Sensitivity of spectral reflectance to variation in live fuel moisture content at leaf and canopy level. *Remote Sens. Environ.* 92 (3), 297–308.
- Brede, B., Verrelst, J., Gastellu-Etchegorry, J.-P., Clevers, J.G.P.W., Goudzwaard, L., den Ouden, J., Verbesselt, J., Herold, M., 2020. Assessment of workflow feature selection on forest LAI prediction with sentinel-2A MSI, Landsat 7 ETM+ and Landsat 8 OLI. *Remote Sensing* 12 (6), 915.
- Breiman, L., 2001. Random forests. *Mach. Learn.* 45, 5–32.
- Broge, N.H., Leblanc, E., 2001. Comparing prediction power and stability of broadband and hyperspectral vegetation indices for estimation of green leaf area index and canopy chlorophyll density. *Remote Sens. Environ.* 76 (2), 156–172.
- Brown, L.A., Ogutu, B.O., Dash, J., 2019. Estimating forest leaf area index and canopy chlorophyll content with Sentinel-2: An evaluation of two hybrid retrieval algorithms. *Remote Sensing* 11 (15), 1752.
- Chen, J.M., Black, T.A., 1992. Defining Leaf Area Index for Non-flat Leaves. *Plant, Cell Environ.* 15 (4), 421–429.
- Chen, J.M., Cihlar, J., 1996. Retrieving leaf area index of boreal conifer forests using Landsat TM images. *Remote Sens. Environ.* 55 (2), 153–162.
- Chen, J.M., 1996. Evaluation of Vegetation Indices and a Modified Simple Ratio for Boreal Applications. *Canadian Journal of Remote Sensing* 22 (3), 229–242.
- Chen, Z., Jia, K., Xiao, C., Wei, D., Zhao, X., Lan, J., Wei, X., Yao, Y., Wang, B., Sun, Y., Wang, L., 2020. Leaf Area Index Estimation Algorithm for GF-5 Hyperspectral Data Based on Different Feature Selection and Machine Learning Methods. *Remote Sensing* 12 (13), 2110.
- Clevers, J., Gitelson, A.A., 2013. Remote estimation of crop and grass chlorophyll and nitrogen content using red-edge bands on sentinel-2 and -3. *Int. J. Appl. Earth Obs. Geoinf.* 23, 344–351.

- Cui, B., Zhao, Q.J., Huang, W.J., Song, X.Y., Ye, H.C., Zhou, X.F., 2019. A new integrated vegetation index for the estimation of winter wheat leaf chlorophyll content. *Remote Sensing* 11, 974.
- Dash, J., Curran, P.J., 2007. Evaluation of the MERIS terrestrial chlorophyll index (MTCI). *Adv. Space Res.* 39 (1), 100–104.
- Delegido, J., Verrelst, J., Meza, C.M., Rivera, J.P., Alonso, L., Moreno, J., 2013. A red-edge spectral index for remote sensing estimation of green LAI over agroecosystems. *Eur. J. Agron.* 46, 42–52.
- Dong, T.F., Liu, J.G., Qian, B.D., He, L.M., Liu, J.N., Wang, R., Jing, Q., Catherine, C., Heather, McNairn, Jarrett, P., Shi, Y.C., Chen, J.M., Shang, J.L., 2020. Estimating crop biomass using leaf area index derived from Landsat 8 and sentinel-2 data. *ISPRS J. Photogramm. Remote Sens.* 168, 236–250.
- Dordas, C.A., Sioulas, C., 2008. Safflower yield, chlorophyll content, photosynthesis, and water use efficiency response to nitrogen fertilization under rainfed conditions. *Ind. Crops Prod.* 27 (1), 75–85.
- Dorigo, W.A., Zurita-Milla, R., Wit, A., Brazile, J., Singh, R., Schaepman, M.E., 2007. A review on reflective remote sensing and data assimilation techniques for enhanced agroecosystem modeling. *Int. J. Appl. Earth Obs. Geoinf.* 9 (2), 165–193.
- Drusch, M., Del Bello, U., Carlier, S., Colin, O., Fernandez, V., Gascon, F., Hoersch, B., Isola, C., Laberinti, P., Martimort, P., Meygret, A., Spoto, F., Sy, O., Marchese, F., Bargellini, P., 2012. Sentinel-2: EAS's optical high-resolution mission for GMES operational services. *Remote Sens. Environ.* 120, 25–36.
- George, R., Padalia, H., Sinha, S.K., Kumar, A.S., 2018. Evaluation of the use of hyperspectral vegetation indices for estimating mangrove leaf area index in middle Andaman Island. *India. Remote Sensing Letters* 9 (11), 1099–1108.
- Gitelson, A.A., Gritz, J., Merzlyak, M.N., 2003. Relationships between leaf chlorophyll content and spectral reflectance and algorithms for non-destructive chlorophyll assessment in higher plant leaves. *J. Plant Physiol.* 160 (3), 271–282.
- Hasegawa, K., Matsuyama, H., Tsuzuki, H., Sweda, T., 2010. Improving the estimation of leaf area index by using remotely sensed NDVI with BRDF signatures. *Remote Sens. Environ.* 114 (3), 514–519.
- Herrmann, I., Pimstein, A., Karnieli, A., Cohen, Y., Alchanatis, V., Bonfil, D.J., 2011. LAI assessment of wheat and potato crops by venus and Sentinel-2 bands. *Remote Sens. Environ.* 115 (8), 2141–2151.
- Jay, S., Maupas, F., Bendoula, R., Gorretta, N., 2017. Retrieving LAI, chlorophyll and nitrogen contents in sugar beet crops from multi-angular optical remote sensing: Comparison of vegetation indices and PROSAIL inversion for field phenotyping. *Field Crops Research* 210, 33–46.
- Jia, K., Liang, S.L., Gu, X.F., Baret, F., Wei, X.Q., Wang, X.X., Yao, Y.J., Yang, L.Q., Li, Y.W., 2016. Fractional Vegetation Cover Estimation Algorithm for Chinese GF-1 Wide Field View Data. *Remote Sens. Environ.* 177, 184–191.
- Jiang, Z., Huete, A.R., Didan, K., Miura, T., 2008. Development of a two-band enhanced vegetation index without a blue band. *Remote Sens. Environ.* 112 (10), 3833–3845.
- Jin, X., Li, Z., Feng, H., Xu, X., Yang, G., 2014. Newly Combined Spectral Indices to Improve Estimation of Total Leaf Chlorophyll Content in Cotton. *IEEE J. Sel. Top. Appl. Earth Obs. Remote Sens.* 7 (11), 4589–4600.
- Rondeaux, G., Steven, M., Baret, F., 1996. Optimization of soil-adjusted vegetation indices. *Remote Sens. Environ.* 55 (2), 95–107.
- Rouse, J.W., Haas, R.H., Jr. Schell, J.A., & Deering, D.W. (1974). Monitoring vegetation systems in the Great Plains with ERTS. Texas A&M Univ., College Station, TX, USA, Tech. Rep. PAPER-A20, 1974.
- Sibanda, M., Mutanga, O., Dube, T., S Vundla, T., & I Mafongoya, P. (2019). Estimating LAI and mapping canopy storage capacity for hydrological applications in wattle infested ecosystems using Sentinel-2 MSI derived red edge bands. *GIScience & Remote Sensing*, 56(1), 68–86.
- Sims, D.A., Gamon, J.A., 2002. Relationships between Leaf Pigment Content and Spectral Reflectance across a Wide Range of Species, Leaf Structures and Developmental Stages. *Remote Sens. Environ.* 81 (2–3), 337–354.
- Sinha, S.K., Padalia, H., Dasgupta, A., Verrelst, J., Rivera, J.P., 2020. Estimation of leaf area index using PROSAIL based LUT inversion, MLRA-GPR and empirical models: Case study of tropical deciduous forest plantation, North India. *Int. J. Appl. Earth Obs. Geoinf.* 86, 102027.
- Sun, Y.H., Qin, Q.M., Ren, H.Z., Zhang, T.Y., Chen, S.S., 2020. Red-Edge Band Vegetation Indices for Leaf Area Index Estimation from Sentinel-2/MSI Imagery. *IEEE Trans. Geosci. Remote Sens.* 58 (2), 826–840.
- Xia, M., Jia, K., Zhao, W.W., Liu, S.L., Wei, X.Q., Wang, B., 2021. Spatio-temporal changes of ecological vulnerability across the Qinghai-Tibetan Plateau. *Ecol. Ind.* 123, 107274.
- Xie, Q.Y., Dash, J., Huang, W.J., Peng, D.L., Qin, Q.M., Mortimer, H., Casa, R., Pignatti, S., Laneve, G., Pascucci, S., Dong, Y.Y., Ye, H.C., 2018. Vegetation Indices Combining the Red and Red-Edge Spectral Information for Leaf Area Index Retrieval. *IEEE J. Sel. Top. Appl. Earth Obs. Remote Sens.* 11 (5), 1482–1492.
- Yan, G.J., Hu, R.H., Luo, J.H., Weiss, M., Jiang, H.L., Mu, X.H., Xie, D.H., Zhang, W.M., 2019. Review of indirect optical measurements of leaf area index: Recent advances, challenges, and perspectives. *Agricultural and Forest Meteorology* 265, 390–411.
- Zhang, Y., Yang, J., Liu, X., Du, L., Shi, S., Sun, J., Chen, B., 2020. Estimation of Multi-Species Leaf Area Index Based on Chinese GF-1 Satellite Data Using Look-up Table and Gaussian Process Regression Methods. *Sensors* 20 (9), 2460.
- Vazquez-Cruz, M.A., Guzman-Cruz, R., Lopez-Cruz, I.L., Cornejo-Perez, O., Torres-Pacheco, I., Guevara-Gonzalez, R.G., 2014. Global Sensitivity Analysis by Means of EFASST and Sobol' Methods and Calibration of Reduced State-Variable TOMGRO Model Using Genetic Algorithms. *Comput. Electron. Agric.* 100, 1–12.